

# Putting 3D Spatially Sparse Networks on a Diet

Junha Lee<sup>1</sup> Christopher Choy<sup>2</sup> Jaesik Park<sup>1</sup>  
POSTECH<sup>1</sup> NVIDIA<sup>2</sup>

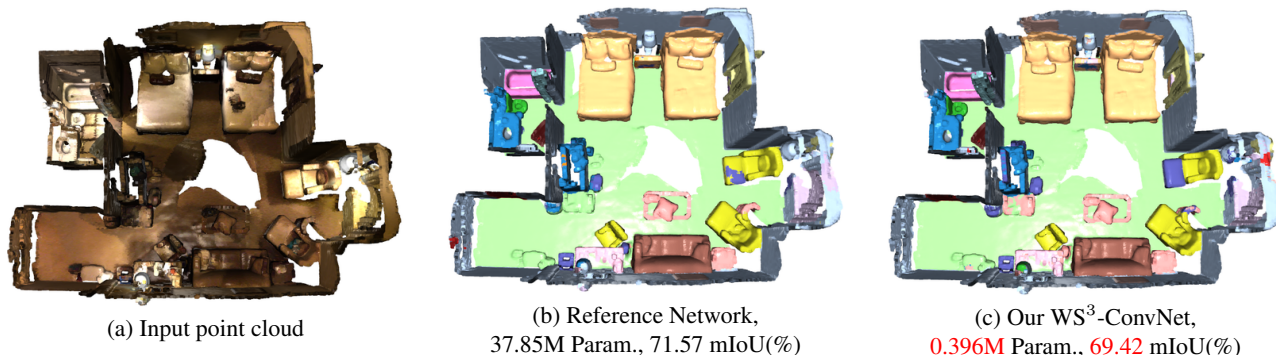


Figure 1. Visualization of semantic label prediction of reference neural network (middle) and our WS<sup>3</sup>-ConvNet that is obtained by pruning 99% of the weights from the reference neural network (right). While the pruned model has 100 times smaller parameters, the mIoU over the entire ScanNet [6] validation split is 69.42%, only the 2.15% drops.

## Abstract

3D neural networks have become prevalent for many 3D vision tasks including object detection, segmentation, registration, and various perception tasks for 3D inputs. However, due to the sparsity and irregularity of 3D data, custom 3D operators or network designs have been the primary focus of 3D research, while the size of networks or efficacy of parameters has been overlooked. In this work, we perform the first comprehensive study on the weight sparsity of spatially sparse 3D convolutional networks and propose a compact weight-sparse and spatially sparse 3D convnet (WS<sup>3</sup>-ConvNet) for semantic segmentation and instance segmentation. We employ various network pruning strategies to find compact networks and show our WS<sup>3</sup>-ConvNet achieves minimal loss in performance (2.15% drop) with orders-of-magnitude smaller number of parameters (1/100 compression rate). Finally, we systematically analyze the compression patterns of WS<sup>3</sup>-ConvNet and show interesting emerging sparsity patterns common in our compressed networks to further speed up inference.

## 1. Introduction

Recent advances in 3D neural networks made various 3D vision applications such as 3D shape classification [31, 32], semantic segmentation [4], object detection [10, 30], reconstruction [25], 3D registration [3, 5], and many other tasks

accessible. These work focus on broadening the spectrum of the 3D neural networks, but, over the years, the majority of research on 3D perception focus more on introducing customized convolution kernels that preserve the continuity of point cloud [24, 31, 32, 37, 38, 40, 47]. However, these continuous convolutions sometimes show lower performance or slower processing time on large scale datasets such as ScanNet [6] or autonomous driving datasets [2, 34] due to the slow and memory intensive nearest neighbor search in 3D. Specifically, to accelerate the nearest neighbor search on GPU, they use pairwise distance computation that is expensive and requires quadratic  $\mathcal{O}(N^2)$  memory footprint. This limits the resolution of the point cloud and prevents wider adoption on large-scale 3D perception.

Discretized convolutions, on the other hand, sacrifice small quantization error ( $\sim 1$ cm) for scalability that can process millions of points with faster inference using the spatially sparse representation and GPU hash tables [4, 9, 10]. Thus, they show promising results on many large-scale indoor [1, 6] and outdoor perception tasks [2, 34]. These discrete convolutions are effective in processing large-scale point clouds, yet these networks are still bulky due to their 3D convolution kernels, preventing wide adoption on edge devices, commodity servers, and low-power devices.

In the image domain, we observe significant advances in network pruning techniques that compress a network by removing redundant parameters [7, 8, 19, 20, 26, 27] and net-

work architecture design methods that reduce the memory and computation cost of a network by introducing efficient architectures [15, 35, 46]. Compared with more mature research in 2D network compression, the network pruning and compression of 3D convnets have rarely been studied except for pruning spatially dense 3D convolution kernels for 2D videos [41].

In this work, to the best of our knowledge, we conduct the first comprehensive study on weight pruning of spatially sparse 3D convolutional networks and create Weight-Sparse and Spatially Sparse 3D convolutional networks (WS<sup>3</sup>-ConvNet). We extensively employ the network pruning methods [7, 11, 20, 26] on two indoor datasets (ScanNet [6] and S3DIS [1]). For each dataset, we prune networks for 1) semantic segmentation networks and 2) instance segmentation networks creating four distinct tasks for network compression. Specifically, we use six pruning methods with three backbone network architectures to find compact 3D neural networks. In total, it requires 5800 hours of GPU computation on 30 GPUs for us to find the optimal pruning setting for 3D network compression. The most effective networks we found show 1/100 compression rate with a negligible drop in performance on 3D perception tasks. We name these networks **WS<sup>3</sup>-ConvNet**.

In addition, we propose the weight-sparse spatially sparse convolution (WS<sup>3</sup>-conv) algorithm. Network compression results in smaller networks and reduction in memory footprint, but faster inference requires dedicated software. Our WS<sup>3</sup>-conv algorithm shows up to 34% reduction in inference time. Lastly, we analyze compression patterns of WS<sup>3</sup>-ConvNet and propose additional structural pruning on top of the most performant network to further speed up inference.

We summarize our contributions as follows:

- We apply network pruning methods on various 3D spatially sparse convolution networks for the various 3D vision tasks that require 5800 hours of GPU time and propose WS<sup>3</sup>-ConvNet.
- We propose an efficient feed-forward algorithm for our *weight-sparse spatially sparse convolution*, which makes use of the compressed weights for faster inference.
- Analysis of the pruned spatially sparse convnets reveal interesting properties of 3D convnets. 1) Pruning a larger 3D convnet is more effective. 2) The decoder part of a 3D U-net is less significant than the encoder. 3) the pruning patterns reveal that a few spatial convolution kernels have no significance.
- We make use of these observations to apply structural pruning and further speed up our WS<sup>3</sup>-ConvNet.

## 2. Related Work

**Deep neural networks for 3D data.** We limit the scope of our work to spatial 3D data, although many refer to

videos as 3D data, as spatial 3D data requires special operators to handle sparsity and irregularity. MLP-based methods [31, 32, 47] directly process the continuous 3D coordinates of point clouds from 3D sensors using a set of MLPs. Recent approaches [24, 37, 38, 40] define customized convolution kernels that apply a series of local transformations on each point. Sparse voxel-based approaches [4, 9], on the other hand, discretize point clouds into discrete voxels and apply spatially sparse convolution, which is mathematically equivalent to regular dense convolution.

Each group targets different aspects of point cloud perception and there are pros and cons of each category. For instance, MLP-based methods [31, 32] are the fastest and the simplest, but often fail to capture local context; others preserve the continuity of points while requiring expensive nearest neighbor search with quadratic memory complexity on GPU [32, 38, 47]. Voxel-based methods introduce a small quantization error, but discretization provides  $\mathcal{O}(1)$  search speed and  $\mathcal{O}(N)$  memory footprint using GPU hash tables. Also, thanks to the mathematical equivalence to 2D convnets, we could borrow many successful network architectures such as skip-connection [13], batch normalization [18], and U-shaped network [33] from 2D CNNs to 3D spatially sparse CNNs.

**Network compression.** Network pruning or network compression is a technique that removes a portion of weights from a neural network to shrink the size of a network and to reduce the amount of computation required for a forward pass. There are three broad categories of network compression depending on when, where, and how a network is pruned.

1) *Unstructured pruning* removes network weights without a predefined structure. LeCun *et al.* [19] identifies the redundant parameters by analyzing sensitivities of parameters using the second-order derivatives of the objective function. Later work [12, 26] replaced the hessian with the Taylor expansion to relax the computation burden of computing the second-order derivatives. Han *et al.* [11] showed that pruning weights with small magnitude and fine-tuning the pruned network leads to a compact model without incurring large loss in accuracy.

2) *Structured pruning* removes a set of network weights with a specific structure (e.g., prune channels, filters altogether) that could provide gains in computation and inference speed without special hardware or software support. Li *et al.* [21] applied magnitude-based pruning to network filters. Other work [16, 22] learn a scaling factor for each channel and prune an entire channel with a lower magnitude scaling factor. Other approaches [14, 23] find channels that don't contribute to the feature reconstruction.

3) *Pruning at initialization* is a recent network pruning method based on the Lottery Ticket Hypothesis (LTH) [7], which claims that there is a subnetwork within a network

that achieves optimal performance and one can find the sub-network by rewinding parameters that survive pruning to their initial values. Frankle *et al.* [8] use larger architectures by relaxing the restriction of reverting the weights to initial values. Zhou *et al.* [48] show that the difference between the initial weights and fine-tuned weights can be another pruning criterion. The proxies for determining lottery tickets in a data-efficient way have been recently studied extensively as well. SNIP [20] aims to find performant subnetworks with a few mini-batch iterations. GraSP [39] and SynFlow [36] suggest that analyzing gradient-flow between layers enables identifying lottery tickets with a small set of training data or even without data.

Note that all of the pruning methods we discussed above mainly focus on 2D perception, i.e., image classification. There is a compression work on dense 3D ConvNets [42], but it is for video understanding to find spatiotemporal features not for spatial 3D data. Hence, to the best of our knowledge, we use network compression methods for spatially sparse 3D neural networks for the first time for 3D perception.

Among the various categories of pruning methods, we mainly use *unstructured pruning* since it is the most effective in finding highly compressed networks that have order-of-magnitude smaller parameters, which is a critical factor for 3D convnet compression. Also, it can be applied to generic network architectures due to its simplicity, is simpler to implement, and can provide insights into structural properties from the final pruning patterns.

### 3. Preliminary

Perception for spatial 3D data such as LiDAR point clouds or RGB-D scans requires non-standard operators that are not provided in the most off-the-shelf neural network libraries to handle sparsity and irregularity of 3D data and to implement fast and efficient local aggregation functions. There are many representations and local aggregation functions, but in this work we focus on spatially sparse convnets. So, we cover the basics of a sparse tensor and spatially sparse convolution in this section.

A **sparse tensor** is the most common data structure for high-dimensional sparse data representation. It assumes that the majority of the data is 0 and saves only the non-zero elements by representing them as their coordinates and values. For high-dimensional tensors, the coordinate format (COO) is the most easy-to-use and versatile representation and we follow the convention. Formally, a  $D + 1$  dimensional spatial sparse tensor consists of  $D$  spatial dimensions and one dense feature dimension. Such sparse tensor with  $N$  non-zero elements can be expressed as follows:

$$\mathcal{T} = (\mathbf{C}, \mathbf{F}), \quad (1)$$

where  $\mathbf{C} \in \mathbb{Z}^{N \times D}$  is row-wise concatenation of discretized

Methods	Neighbor Search		Large-scale Inference	Latency (Sec.)
	Preparation	Inference		
KPCConv <i>deform</i> [38]	$\mathcal{O}(N \log N)$	$\mathcal{O}(KM \log N)$	Crop & Stitch	105.15
PAConv [44]	$\mathcal{O}(1)$	$\mathcal{O}(MN \log K)$	Crop & Stitch	28.13
PointTransformer [47]	$\mathcal{O}(1)$	$\mathcal{O}(MN \log K)$	Multi-shot	18.07
Res16UNet34C	$\mathcal{O}(N)$	$\mathcal{O}(M)$	Single-shot	0.07

Table 1. Run time comparison. We analyze the theoretical time complexity of neighbor search algorithms and evaluate per-scene wall-time latency of each network. We denote  $N$  as # of dataset points,  $M$  as # of query points, and  $K$  as # of neighbors to search. Both  $M$  and  $N$  are much larger than  $K$  in a large-scale point cloud. We use S3DIS [1] Area 5 test scene with a single Geforce RTX 3090 GPU for the comparison.

coordinates, and  $\mathbf{F} \in \mathbb{R}^{N \times N_F}$  is corresponding feature vectors of size  $N_F$ . We will use  $\mathbf{C}$  to denote a set of non-zero coordinates and a coordinate matrix, but it will be clear from the context.

**Spatially sparse convolution** is a generalized version of the conventional dense convolution so that it can operate on a sparse tensor. Given an input sparse tensor at  $l$ -th layer,  $\mathcal{T}^l = (\mathbf{C}^l, \mathbf{F}^l)$  where  $\mathbf{C}^l \in \mathbb{Z}^{N \times D}$  denotes the  $D$ -dimensional coordinates, and  $\mathbf{F}^l \in \mathbb{R}^{N \times N_F^l}$  denotes corresponding features. The spatially sparse convolution is defined as follows:

$$\mathbf{f}_c^{l+1} = \sum_{i \in \mathcal{K}(\mathbf{c})} \mathbf{W}_i^l \cdot \mathbf{f}_{c+i}^l, \quad (2)$$

where  $\mathbf{f}_c^l \in \mathbb{R}^{N_F^l}$  is a feature vector at coordinate  $\mathbf{c}$ ,  $\mathbf{W} \in \mathbb{R}^{K^D \times N_F^{l+1} \times N_F^l}$  is the kernel weights with kernel size  $K$ ,  $\mathbf{c} \in \mathbb{Z}^D$  is the current position of kernel center, and  $\mathcal{K}(\mathbf{c})$  denotes a list of offsets in  $D$ -dimensional hypercube centered at  $\mathbf{c}$ . The convolution kernel,  $\mathcal{K}(\cdot)$ , is applied only on non-zero elements as the rest of the input is 0.

**Neighbor search**, where a convolution kernel finds non-zero neighbors within the current receptive field around  $\mathbf{c}$  ( $\mathcal{K}(\mathbf{c})$ ), is one of the areas the spatially sparse convolution shows its effectiveness and scalability. It uses a GPU hash table to speed up the search with  $\mathcal{O}(1)$  complexity, which differentiates itself with other approaches that use continuous points and  $\mathcal{O}(N^2)$  memory complexity for neighbor search [24, 31, 32, 38, 47].

Note that continuous convolution methods [38, 44, 47] require multiple crops with a sliding window to handle large-scale scenes. Such sliding window makes them a few orders of magnitude slower than hash-table based neighbor search of spatially sparse convolution.

**Spatial sparsity vs. weight sparsity.** The 3D convolutions are bulkier than 2D networks due to the extra spatial dimension. Note that in 2D, there are  $K^2$  weight matrices of size  $N_F^{l+1} \times N_F^l$  where  $K$  is the kernel size, but in 3D, it requires  $K^3$  weight matrices. Thus, to reduce the

number of parameters, we prune some of the weights from the convolution filters by applying successful pruning approaches [7, 8, 11, 12, 19, 20, 26]. As a result, the pruned network has sparse weights, and we use them for convolution. To revisit Eq. 2, we prune the weight matrix  $W_i$  and convert it to a sparse matrix. However, the convolution is applied only on spatially sparse coordinates  $C$ .

## 4. Spatially Sparse Network Compression

Compressing a neural network requires first training a neural network with dense weights. We first discuss the target tasks and the training procedure in Section 4.1. Next, we introduce pruning methods we adopt in Section 4.2 and discuss the pruning procedure. In Section 4.3, we use the compressed spatially sparse convnet or weight-sparse spatially sparse convnet (WS<sup>3</sup>-ConvNet) for faster inference by introducing our weight-sparse convolution algorithm.

### 4.1. Training Spatially Sparse ConvNets

To achieve high performance and good network compression rate, neural network has to be fine-tuned on a specific task. We define two most common 3D tasks for our network compression that are practical and computationally demanding: semantic segmentation and instance segmentation. For all experiments, we use U-shaped fully convolutional networks with residual blocks as depicted in Figure 2 (top). For the last layer, we use logit prediction per voxel for semantic segmentation. For instance segmentation, we use logits with object center offset prediction as two outputs. We use a pytorch spatially sparse convolution implementation for all training [4].

We follow the standard training procedure in [4], but do not apply any rotation averaging, or more advanced data augmentation techniques [28] to compare our network fairly with other methods that use the same datasets. We use cross-entropy loss for semantic segmentation:

$$\mathcal{L}_{\text{sem}} = -\frac{1}{N} \sum_{n=1}^N \sum_{c=1}^C y_{n,c} \log(p_{n,c}), \quad (3)$$

and for instance segmentation, we use the auxiliary loss for regressing the object center offset as follows:

$$\mathcal{L}_{\text{ins}} = \mathcal{L}_{\text{sem}} + \frac{1}{N} \sum_{n=1}^N \left( |c_n - c_n^*| - \frac{c_n \cdot c_n^*}{\|c_n\| \|c_n^*\|} \right). \quad (4)$$

We train total three variants of networks with various depths and widths and train them with the same training procedure. The detailed configuration of each network and the training parameters can be found in Section 5.2 and the supplementary material.

---

### Algorithm 1: Iterative Pruning Algorithm.

---

**Input:**  $\mathcal{F}(\cdot, \theta_{\text{init}})$ : a pre-trained net. with param.  $\theta_{\text{init}}$ .  
 $i_{\text{train}}$ : number of training iterations.  
 $i_{\text{prune}}$ : number of fine-tuning iterations per step.  
 $N_{\text{prune}}$ : number of pruning iteration to repeat.  
 $p_{\text{target}}$ : target pruning ratio.  
**criteria**( $\cdot$ ): a score function for pruning.  
**Output:**  $\theta'$ : a pruned network parameter.

```

1 function IterativePruning
2    $\theta \leftarrow \theta_{\text{init}}$ 
3    $m \leftarrow \text{ones\_like}(\theta)$  // init. pruning mask
4    $p \leftarrow 1 - (1 - p_{\text{target}})^{\frac{1}{N_{\text{prune}}}}$ 
5   for  $i \leftarrow 1$  to  $i_{\text{train}}$  do
6     if  $i \% i_{\text{prune}} == 0$  then
7        $s \leftarrow \text{criteria}(\theta \odot m)$  // score
8        $\text{idx} \leftarrow \text{argsort}(s, p)$  // sort
9        $m[\text{idx}] \leftarrow 0$  // update mask
10    else
11       $\theta \leftarrow \text{train}(\mathcal{F}(\cdot, \theta \odot m))$  // fine-tune
12    end
13  end
14  return  $\theta' \leftarrow \theta$ 
15 end

```

---

Tag	Approach	Pruning criteria	Scope
L1L	L1	$ \mathbf{w}_f $	Local
L1G	L1	$ \mathbf{w}_f $	Global
FGL	First-order grad.	$\left  \frac{\partial \mathcal{L}}{\partial \mathbf{w}} \odot \mathbf{w}_f \right $	Local
FGG	First-order grad.	$\left  \frac{\partial \mathcal{L}}{\partial \mathbf{w}} \odot \mathbf{w}_f \right $	Global
L1SL	L1 w/ same sign	$\frac{ \mathbf{w}_0 }{ \mathbf{w}_0 } \cdot \mathbf{w}_f$	Local
L1SG	L1 w/ same sign	$\frac{ \mathbf{w}_0 }{ \mathbf{w}_0 } \cdot \mathbf{w}_f$	Global

Table 2. Set of pruning strategies applied to the baseline models. We consider three different pruning criteria with *Local* and *Global* scope, which results in total six combinations. Here,  $\mathcal{L}$  denotes the objective function,  $\mathbf{w}_0$  is the initial, pretrained weights, and  $\mathbf{w}_f$  denotes the weights that can be obtained after fine-tuning.

### 4.2. Network Pruning

Once we finish training a spatially sparse convnet with dense weights, we prune some of the weights while preserving the test accuracy. In this paper, we utilize several pruning methods that belong to the family of magnitude-based pruning [7, 11, 20, 48]. Specifically, we use three pruning methods with different pruning criteria and apply the criteria on the entire weights (global) or per layer (local). We put all our pruning criteria on Table 2. Starting from a pre-trained model, we cycle through a series of the network pruning and fine-tuning iteratively. At each pruning step, we use the pruning criteria to sort the weights and remove lower  $p$  portion of weights and repeat this  $N_{\text{prune}}$  times so the final target pruning rate is  $p_{\text{target}} = 1 - (1 - p)^{N_{\text{prune}}}$ , where  $p$  and  $N_{\text{prune}}$  are predefined hyperparameters.

We apply each pruning method to each pre-trained network with the same target compression rate to compare the effect of different pruning criteria. All hyperparameters other than pruning strategies, e.g., number of fine-tuning steps between consecutive pruning steps, learning rates, etc., are set to be the same for every model and a pruning strategy pair. We put our pruning procedure on Algorithm 1.

### 4.3. Weight-Sparse Spatially Sparse Convolution

Network compression of spatially sparse convnets results in highly compressed networks with minimal loss in accuracy. This leads to the reduction in memory footprint and faster transfer, but, faster inference requires dedicated software to make use of the compressed convolution kernels and the computational reduction from pruning. To this end, we extend a pytorch spatially sparse convolution library [4] with a specialized convolution layer for weight-sparse spatially sparse convolution (WS<sup>3</sup>-convolution).

The WS<sup>3</sup>-convolution consists of several steps:

- *Kernel mapping*: The spatially sparse convolution computes convolution only on non-zero elements neighbors. This requires extracting appropriate features from neighbors and placing the result on the center of convolution. This input neighbor to output pair is known as kernel mapping and we use it to select input features.
- *CSR compression*: We compress the dense weight matrices with pruning masks  $m$ . We use the *Compressed Sparse Row* (CSR) format and convert the masked dense weight matrices to sparse matrices.
- *Transposition*: Majority of the off-the-shelf BLAS libraries such as *Intel oneMKL* and *cuSparse* commonly use sparse-dense matrix multiplication routine with the sparse matrix being the left operand. However, the feature maps are represented in memory with row-major layout [4, 29]. Thus, we transpose the feature map for sparse dense multiplication. We pre-transpose weight matrices before the CSR compression.
- *Sparse matrix multiplication*: Finally, we use off-the-shelf libraries to compute temporary features and place the output on the correct position defined by the kernel mapping.

We put the detailed algorithm on Algorithm 2.

## 5. Experiment

In this section, we present the results and analysis of our network pruning experiments that require in total 5800 hours of GPU computation on 30 GPUs.

### 5.1. Experiment setup and metrics

We use semantic segmentation and instance segmentation on two indoor datasets for the compression of spatially

---

### Algorithm 2: Weight-Sparse Convolution Algorithm.

---

**Input:**  $\mathcal{T}_{in} = \{\mathbf{C}, \mathbf{F}\}$ : an input sparse tensor with coordinates in COO layout.  
 $\mathbf{C} \in \mathbb{Z}^{N \times 3}$  is non-zero discrete coordinates.  
 $\mathbf{F} \in \mathbb{R}^{N \times N_{in}}$  is a feature map of  $\mathbf{C}$ .  
 $\mathbf{W} \in \mathbb{R}^{K \times N_{out} \times N_{in}}$ : the weight tensor of sparse convolution layer with kernel size  $K$ , input feature dimension  $N_{in}$ , output dimension  $N_{out}$

**Output:**  $\mathcal{T}_{out} = \{\mathbf{C}, \mathbf{F}'\}$ : the output sparse tensor.

```

1 function Weight-Sparse Convolution
  // construct kernel in-out map
2  $\mathcal{K}(\cdot) \leftarrow \text{constructKernelInOutMap}(\mathbf{C}, K)$ 
  // compress weights to CSR layout
3  $\mathbf{W}_{sp}^T \leftarrow \text{compress}(\text{transpose}(\mathbf{W}))$ 
  // initialize output features map
4  $\mathbf{F}_{out} \leftarrow \text{zeros}(\text{shape} = \{N, N_{out}\})$ 
5 for  $k \leftarrow 1$  to  $K^3$  do
  // retrieve kernel in-out map
6  $(\mathcal{K}_{in}, \mathcal{K}_{out}) \leftarrow \text{retrieveInOutMap}(\mathbf{C}, k)$ 
  // transpose matrices
7  $\mathbf{F}_{in}^T \leftarrow \text{transpose}(\mathbf{F}[\mathcal{K}_{in}, :])$ 
  // sparse-dense matmul
8  $\mathbf{F}_{out}[\mathcal{K}_{out}] += \text{transpose}(\mathbf{W}_{sp,k}^T @ \mathbf{F}_{in}^T)$ 
9 end
10  $\mathcal{T}_{out} \leftarrow \{\mathbf{C}, \mathbf{F}_{out}\}$ 
11 return  $\mathcal{T}_{out}$ 
12 end
```

---

sparse convnets. ScanNet [6] consists of 1.5k scenes captured with commercial RGB-D cameras. It provides diverse indoor scenes but exhibits incomplete reconstruction and occlusion. On the other hand, the S3DIS [1] dataset provides 271 indoor office rooms captured with LiDAR 3D scanning devices. The reconstruction is complete and well aligned, but the scenes are monotonic compared with ScanNet.

We measure the intersection of union (IoU) and per-point classification accuracy for each semantic class, and report the mean IoUs (mIoU), and mean accuracy (mAcc) for semantic segmentation. For instance segmentation, we report average precision per class and mean average precision with varying accuracies 50% and 25% which we denote as mAP50 and mAP25 respectively.

We use three different network architectures with varying depth and width: Res16UNet14A, Res16UNet18A, Res16UNet34C [4]. We apply unstructured pruning [7, 11, 20, 48] and compare the results with representative point-based approaches [31, 32, 37, 38, 43–45, 47].

### 5.2. Implementation detail

We train all our networks for 60K iterations with an initial learning rate 0.1, 2cm voxelization, and batch size 8 on both datasets. After the baseline networks are converged,

	# Param.(M)	Rel.(%)	ScanNet [6]				S3DIS [1]			
			mIoU(%)	Rel.(%)	mAcc(%)	Rel.(%)	mIoU(%)	Rel.(%)	mAcc(%)	Rel.(%)
PointNet [31]	3.5	↓ 56.6	12.2	↓ 82.2	17.9	↓ 77.0	41.1	↓ 37.8	49.0	↓ 34.6
PointNet++ [32]	2.0	↓ 75.2	53.5	↓ 21.9	-	-	57.3	↓ 13.3	63.5	↓ 15.3
TangentConv [37]	1.0	↓ 87.4	40.9	↓ 40.3	55.1	↓ 29.1	52.8	↓ 20.1	62.2	↓ 17.0
PointConv [43]	-	-	61.0	↓ 11.0	-	-	-	-	-	-
PointASNL [45]	-	-	63.5	↓ 7.31	-	-	-	-	-	-
KPConv [38]	14.9	↑ 85.9	69.2	↑ 1.01	-	-	67.1	↑ 1.53	72.8	↓ 2.87
PACConv [44]	11.8	↑ 47.2	-	-	-	-	66.6	↑ 0.77	73.0	↓ 2.60
PointTransformer [47]	7.8	↓ 2.67	-	-	-	-	70.4	↑ 6.52	76.5	↑ 2.07
Res16UNet14A	8.0	±0.00	68.5	±0.00	77.7	±0.00	66.1	±0.00	75.0	±0.00
└ 90% pruning rate	0.8	↓ 89.9	67.9	↓ 0.95	77.3	↓ 0.53	65.1	↓ 1.48	72.0	↓ 3.90
└ 95% pruning rate	0.4	↓ 94.9	67.2	↓ 1.96	76.9	↓ 1.08	64.8	↓ 1.91	72.2	↓ 3.64
└ 99% pruning rate	0.1	↓ 98.9	59.3	↓ 13.4	70.3	↓ 9.46	60.9	↓ 7.87	68.7	↓ 8.35
Res16UNet18A	15.5	↑ 93.4	70.3	↑ 2.58	79.7	↑ 2.54	67.6	↑ 2.30	74.6	↓ 0.51
└ 90% pruning rate	1.6	↓ 80.6	69.9	↑ 2.03	79.0	↑ 1.72	66.5	↑ 0.57	73.0	↓ 2.60
└ 95% pruning rate	0.8	↓ 90.2	69.3	↑ 1.09	78.6	↑ 1.20	66.3	↑ 0.30	73.2	↓ 2.32
└ 99% pruning rate	0.2	↓ 97.9	65.7	↓ 4.10	76.1	↓ 2.03	64.2	↓ 2.84	71.4	↓ 4.68
Res16UNet34C	37.9	↑ 372.9	71.6	↑ 4.47	80.4	↑ 3.53	68.8	↑ 4.04	75.8	↑ 1.17
└ 90% pruning rate	3.8	↓ 52.6	71.0	↑ 3.68	79.8	↑ 2.70	66.5	↑ 0.59	73.1	↓ 2.44
└ 95% pruning rate	1.9	↓ 76.2	71.0	↑ 3.56	79.7	↑ 2.63	66.4	↑ 0.48	73.2	↓ 2.31
└ 99% pruning rate	0.4	↓ 95.1	69.5	↑ 1.40	78.9	↑ 1.60	65.7	↓ 0.67	72.8	↓ 2.92

Table 3. Quantitative results of *semantic segmentation* models on ScanNet [6] and S3DIS dataset [1]. Gray row indicates the reference network, and we color green for the **positive changes** and red for the **negative changes** w.r.t. the reference network.

	# Param.(M)	Rel.(%)	ScanNet [6]				S3DIS [1]			
			mAP50(%)	Rel.(%)	mAP25(%)	Rel.(%)	mAP50(%)	Rel.(%)	mAP25(%)	Rel.(%)
Res16UNet14A	8.0	±0.00	52.8	±0.00	68.1	±0.00	54.5	±0.00	61.7	±0.00
└ 90% pruning rate	0.8	↓ 89.9	51.2	↓ 3.03	66.4	↓ 2.50	48.7	↓ 10.6	60.7	↓ 1.62
└ 95% pruning rate	0.4	↓ 94.9	48.9	↓ 7.39	65.4	↓ 3.96	48.7	↓ 10.6	59.4	↓ 3.73
└ 99% pruning rate	0.1	↓ 98.9	34.6	↓ 34.5	55.9	↓ 17.9	37.7	↓ 30.8	52.2	↓ 15.4
Res16UNet18A	15.5	↑ 93.3	55.8	↑ 5.68	71.3	↑ 4.70	55.6	↑ 2.02	62.7	↑ 1.62
└ 90% pruning rate	1.6	↓ 80.5	55.7	↑ 5.49	71.8	↑ 5.43	48.5	↓ 11.0	59.6	↓ 3.40
└ 95% pruning rate	0.8	↓ 90.2	55.5	↑ 5.11	71.2	↑ 4.55	49.8	↓ 8.62	58.7	↓ 4.86
└ 99% pruning rate	0.2	↓ 97.9	47.3	↓ 10.4	65.3	↓ 4.11	45.1	↓ 17.2	56.6	↓ 8.27
Res16UNet34C	37.9	↑ 372.6	57.0	↑ 7.95	73.1	↑ 7.34	54.7	↑ 0.37	64.1	↑ 3.89
└ 90% pruning rate	3.8	↓ 52.6	56.9	↑ 7.77	71.7	↑ 5.29	48.3	↓ 11.4	59.4	↓ 3.73
└ 95% pruning rate	1.9	↓ 76.2	56.3	↑ 6.63	71.5	↑ 4.99	51.0	↓ 6.42	60.0	↓ 2.76
└ 99% pruning rate	0.4	↓ 95.0	54.2	↑ 2.65	71.0	↑ 4.26	48.9	↓ 10.3	58.4	↓ 5.35

Table 4. Quantitative results of *instance segmentation* models on ScanNet [6] and S3DIS dataset [1]. Gray row indicates the reference network, and we color green for the **positive changes** and red for the **negative changes** w.r.t. the reference network.

we apply our iterative pruning with  $i_{\text{train}} = 60K$  total training iteration, and  $N_{\text{prune}} = 10$  pruning and fine-tuning sequences with  $i_{\text{prune}} = 2K$  fine-tuning iterations between the consecutive pruning sequences for all experiments. All the experiments are evaluated on an NVIDIA Titan RTX and Intel Xeon Gold 5220R.

### 5.3. Experiment Results and Analysis

We compress various backbone networks with multiple pruning rates and present the semantic segmentation results on Table 3 and instance segmentation results on Table 4. We present our analysis of these results in this section.

**Conventional 3D ConvNets are bulky.** On Table 3, we can see that KPConv [38], PACConv [44], and PointTransformer [47] achieve high performance on S3DIS while having as many parameters as Res16UNet14A. However, even when we prune 90% of parameters from Res16UNet14A, the relative performance drop is only 0.5~3.9%. On the other hand, PointNet [31], PointNet++ [32], and TangentConv [37] have almost the same number of parameters as 90% pruned Res16UNet14A. However, the 90% pruned ResNet outperforms these networks by a decent margin. Similarly, PACConv [44] having 11.8M parameters shows comparable results to 90% pruned Res16UNet18A with

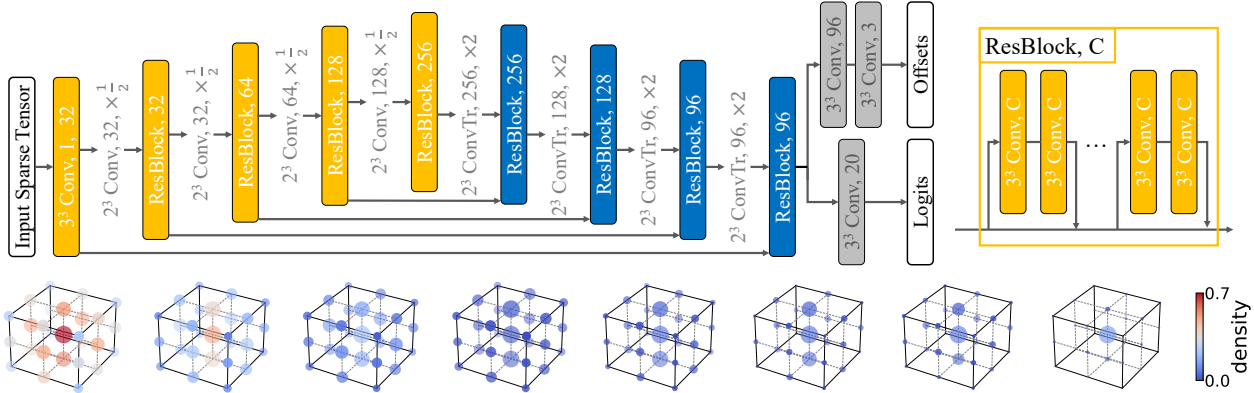


Figure 2. (Top) Res16UNet network architecture. It is a U-shape network with an encoder (yellow) and decoder (blue), and has skip connections. (Bottom) Visualization of compressed convolution kernels. Each grid represents the average density of the first  $3 \times 3 \times 3$  convolution kernel in each residual block from encoder to decoder from left to right. Note that kernels in decoder are pruned more aggressively in general, but weights along z-axis tend to survive.

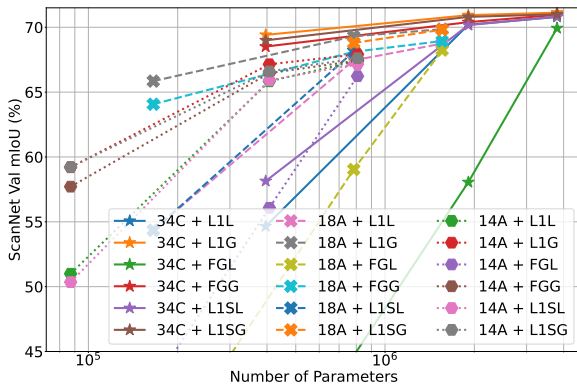


Figure 3. Ablation study on different pruning criteria on ScanNet semantic segmentation. For all architectures, L1G (Global L1 magnitude-based pruning) shows the least drop in performance. We use 34C, 18A, and 14A to denote Res16UNet variants. For pruning method tags, please refer to Table 2.

1.6M parameters.

**Prune overparametrized networks.** Another interesting observation is that we see a small performance drop when we compress heavier networks. For example, in Table 3, Res16UNet14A with a 95% compression (Network A) and Res16UNet34C with a 99% compression (Network B) both have a similar number of parameters. Yet, Network B consistently shows higher accuracy on ScanNet and S3DIS. We speculate that heavier and deeper networks still retain the same depths regardless of compression and overparametrization leads to a higher chance of maintaining more informative connections during pruning.

**Global pruning is better than local pruning.** We visualize the performance vs. network size graph on Figure 3. Global pruning that prunes the entire network weights perform better than local pruning that prunes the same percent-

age of weights from each layer. For instance, ‘34C+L1G’ shows smaller drop in performance than ‘34C+L1L’. This is common in all backbone networks and we will explain this in the next paragraph.

**Decoder of U-Net is overparametrized.** We visualize the pruning patterns of convolution kernels on Figure 2 (bottom). Note that the encoder retains more connections while the decoder is pruned aggressively. This indicates that the decoder has more redundant connections and shows that pruning globally allows the pruning algorithm to choose the importance freely among all layers leading to higher performance than local pruning.

**Kernels along gravity-axis are more important.** Pruning patterns on Figure 2 (bottom) show that kernels along the gravity-axis have higher density than any other directions. We speculate that the vertical geometric patterns are especially important in indoor scenes due to structural similarity and height from the ground is critical in indoor perception.

## 5.4. WS<sup>3</sup>-ConvNet

Based on the experiments and observations, we pick Res16UNet34C network with 99% pruning rate as our representative result, and name it WS<sup>3</sup>-ConvNet. As shown in Table 3, Table 4, Figure 1, and Figure 4, WS<sup>3</sup>-ConvNet shows very high accuracy (69.4% mIoU) with only 0.4M parameters, which is even smaller than PointNet [31] and PointNet++ [32].

In addition, we test our weight-sparse convolution algorithm in Algorithm 2 and measure the speed up on Table 5. Compared with the dense inference time, the sparse time, which measures the inference time for 99% pruned networks, shows up to 34% speedup and the speedup is consistent across tasks and networks.

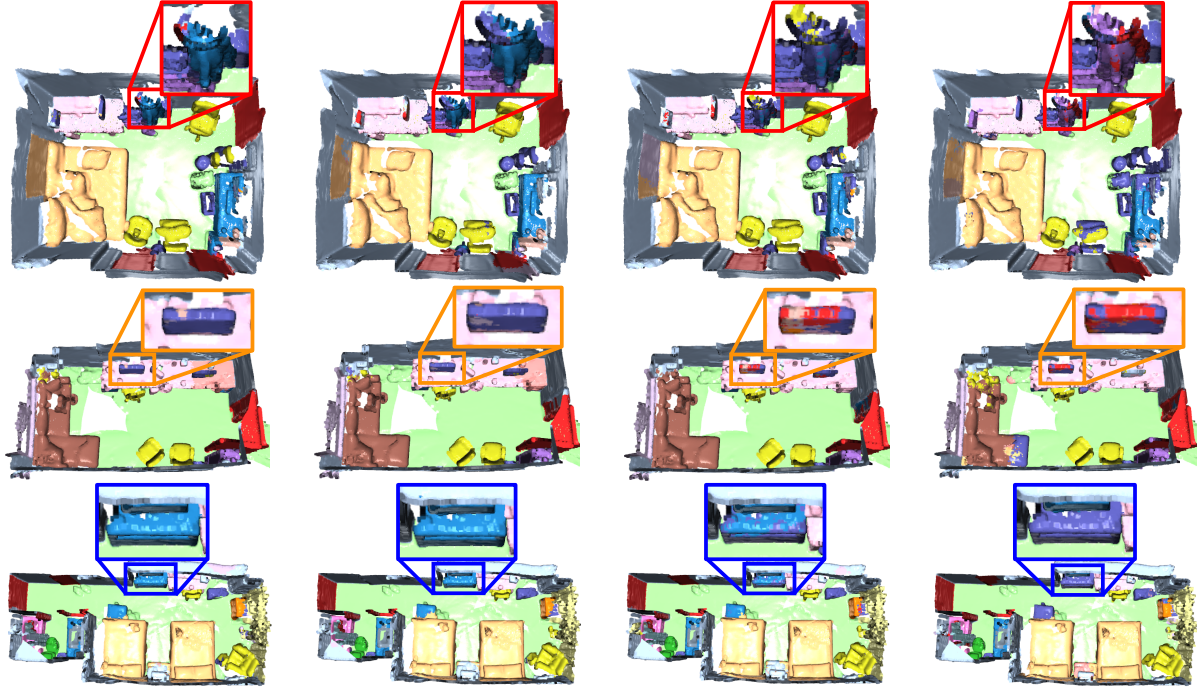


Figure 4. Visualization of semantic segmentation prediction on ScanNet [17] using Res16UNet34C with varying sparsity (Dense, 90%, 95%, and 99% pruned models from left to right).

Arch.	ScanNet [6]			S3DIS [1]		
	Dense time	Sparse time	Rel.(%)	Dense time	Sparse time	Rel.(%)
Semantic Segmentation						
Res16UNet14A	2.63	1.95	↓25.8	1.77	1.23	↓30.3
Res16UNet18A	4.55	3.06	↓32.9	2.83	1.96	↓30.9
Res16UNet34C	4.57	3.25	↓28.8	2.84	2.14	↓24.7
Instance Segmentation						
Res16UNet14A	2.83	1.95	↓31.1	1.78	1.33	↓25.1
Res16UNet18A	4.47	3.20	↓28.4	3.09	2.04	↓33.9
Res16UNet34C	4.70	3.28	↓30.2	3.13	2.13	↓31.8

Table 5. Comparison on the inference speed of *spatially-sparse* convolutional networks and WS<sup>3</sup>-ConvNet. Times are the average latency per scene and measure on CPU. Our implementation of WS<sup>3</sup>-ConvNet exhibits up to 34% reduction of inference time.

## 5.5. Structural Pruning of Spatial Kernels

Lastly, we utilize the fact that, on the decoder side, the convolution kernels along the gravity-axis are more important, and further compress the networks using structural pruning. We *switch-off* the kernels that are y off the z-axis and present the performance drop and speedup in Table 6. Note that switching off kernels in the last few layers doesn't harm the accuracy much, while it enables faster inference.

## 6. Discussion

In this work, we apply various network compression methods on 3D spatially sparse convolutional networks. We found that 3D convnets can be compressed effectively to re-

B1	B2	B3	B4	B5	B6	B7	B8	mIoU(%)	mAcc(%)	Time(s)
								71.6(+3.02)	80.4(+1.90)	4.57(+38.5)
								69.5(±0.00)	78.9(±0.00)	3.30(±0.00)
						✓	✓	69.2(-0.42)	78.8(-0.18)	2.59(-21.6)
						✓	✓	64.3(-7.39)	73.5(-6.90)	2.26(-31.5)
					✓	✓	✓	40.6(-41.6)	46.0(-41.7)	2.12(-35.7)
					✓	✓	✓	11.9(-82.9)	15.7(-80.2)	2.25(-31.9)
					✓	✓	✓	3.65(-94.8)	7.10(-91.0)	2.04(-38.2)
					✓	✓	✓	3.50(-95.0)	6.92(-91.2)	1.92(-42.0)
	✓	✓	✓	✓	✓	✓	✓	2.61(-96.2)	6.03(-92.4)	1.85(-44.1)
✓	✓	✓	✓	✓	✓	✓	✓	5.63(-91.9)	9.73(-87.7)	1.72(-47.8)

Table 6. Ablation study on the effect of z-axis aligned kernels. Columns B1 to B8 indicate residual blocks in our model (Res16UNet34C, 99% pruned), ✓ denotes that the only weights along the z-axis of 3<sup>3</sup> kernel are used to compute output features for all conv layers in the block. All inference time measured on CPU. Gray row indicates the dense (0% pruned) model.

tain only 1% of its original weights while maintaining very high accuracy. Also, to speed up the inference, we propose weight-sparse convolution algorithm and show up to 34% speedup. Analysis shows interesting properties of 3D convnets and we further utilize the findings to apply additional structural pruning.

We only pruned spatially sparse networks, but would like to incorporate other networks for compression. In addition, we only used unstructured pruning but will study the effect of structured pruning and network architecture search (NAS) to find the optimal compressed network.

## References

- [1] Iro Armeni, Ozan Sener, Amir R. Zamir, Helen Jiang, Ioannis Brilakis, Martin Fischer, and Silvio Savarese. 3d semantic parsing of large-scale indoor spaces. In *Proceedings of the IEEE International Conference on Computer Vision and Pattern Recognition*, 2016. [1](#), [2](#), [3](#), [5](#), [6](#), [8](#), [11](#), [12](#), [14](#), [15](#)
- [2] J. Behley, M. Garbade, A. Milioto, J. Quenzel, S. Behnke, J. Gall, and C. Stachniss. Towards 3D LiDAR-based semantic scene understanding of 3D point cloud sequences: The SemanticKITTI Dataset. *The International Journal on Robotics Research*, 40(8-9):959–967, 2021. [1](#)
- [3] Christopher Choy, Wei Dong, and Vladlen Koltun. Deep global registration. In *Proceedings of the IEEE/CVF conference on computer vision and pattern recognition*, pages 2514–2523, 2020. [1](#)
- [4] Christopher Choy, JunYoung Gwak, and Silvio Savarese. 4d spatio-temporal convnets: Minkowski convolutional neural networks. In *Proceedings of the IEEE/CVF Conference on Computer Vision and Pattern Recognition*, pages 3075–3084, 2019. [1](#), [2](#), [4](#), [5](#)
- [5] Christopher Choy, Jaesik Park, and Vladlen Koltun. Fully convolutional geometric features. In *Proceedings of the IEEE/CVF International Conference on Computer Vision*, pages 8958–8966, 2019. [1](#)
- [6] Angela Dai, Angel X Chang, Manolis Savva, Maciej Halber, Thomas Funkhouser, and Matthias Nießner. Scannet: Richly-annotated 3d reconstructions of indoor scenes. In *Proceedings of the IEEE conference on computer vision and pattern recognition*, pages 5828–5839, 2017. [1](#), [2](#), [5](#), [6](#), [8](#), [11](#), [12](#), [14](#)
- [7] Jonathan Frankle and Michael Carbin. The lottery ticket hypothesis: Finding sparse, trainable neural networks. In *International Conference on Learning Representations*, 2019. [1](#), [2](#), [4](#), [5](#)
- [8] Jonathan Frankle, Gintare Karolina Dziugaite, Daniel M Roy, and Michael Carbin. Stabilizing the lottery ticket hypothesis. *arXiv preprint arXiv:1903.01611*, 2019. [1](#), [3](#), [4](#)
- [9] Benjamin Graham. Spatially-sparse convolutional neural networks. *arXiv preprint arXiv:1409.6070*, 2014. [1](#), [2](#)
- [10] JunYoung Gwak, Christopher Choy, and Silvio Savarese. Generative sparse detection networks for 3d single-shot object detection. In *Computer Vision—ECCV 2020: 16th European Conference, Glasgow, UK, August 23–28, 2020, Proceedings, Part IV 16*, pages 297–313. Springer, 2020. [1](#)
- [11] Song Han, Jeff Pool, John Tran, and William J Dally. Learning both weights and connections for efficient neural network. In *NIPS*, 2015. [2](#), [4](#), [5](#)
- [12] Babak Hassibi, David G Stork, and Gregory J Wolff. Optimal brain surgeon and general network pruning. In *IEEE international conference on neural networks*, pages 293–299. IEEE, 1993. [2](#), [4](#)
- [13] Kaiming He, Xiangyu Zhang, Shaoqing Ren, and Jian Sun. Deep residual learning for image recognition. In *Proceedings of the IEEE conference on computer vision and pattern recognition*, pages 770–778, 2016. [2](#)
- [14] Yihui He, Xiangyu Zhang, and Jian Sun. Channel pruning for accelerating very deep neural networks. In *Proceedings of the IEEE international conference on computer vision*, pages 1389–1397, 2017. [2](#)
- [15] Andrew G Howard, Menglong Zhu, Bo Chen, Dmitry Kalenichenko, Weijun Wang, Tobias Weyand, Marco Andreetto, and Hartwig Adam. Mobilenets: Efficient convolutional neural networks for mobile vision applications. *arXiv preprint arXiv:1704.04861*, 2017. [2](#)
- [16] Zehao Huang and Naiyan Wang. Data-driven sparse structure selection for deep neural networks. In *Proceedings of the European conference on computer vision (ECCV)*, pages 304–320, 2018. [2](#)
- [17] Forrest N Iandola, Song Han, Matthew W Moskewicz, Khalid Ashraf, William J Dally, and Kurt Keutzer. Squeezenet: Alexnet-level accuracy with 50x fewer parameters and 0.5 mb model size. *arXiv preprint arXiv:1602.07360*, 2016. [8](#)
- [18] Sergey Ioffe and Christian Szegedy. Batch normalization: Accelerating deep network training by reducing internal covariate shift. In *International conference on machine learning*, pages 448–456. PMLR, 2015. [2](#)
- [19] Yann LeCun, John S Denker, and Sara A Solla. Optimal brain damage. In *NIPS*, pages 598–605, 1990. [1](#), [2](#), [4](#)
- [20] Namhoon Lee, Thalaiyasingam Ajanthan, and Philip Torr. Snip: Single-shot network pruning based on connection sensitivity. In *International Conference on Learning Representations*, 2018. [1](#), [2](#), [3](#), [4](#), [5](#)
- [21] Hao Li, Asim Kadav, Igor Durdanovic, Hanan Samet, and Hans Peter Graf. Pruning filters for efficient convnets. *International Conference on Learning Representations*, 2017. [2](#)
- [22] Zhuang Liu, Jianguo Li, Zhiqiang Shen, Gao Huang, Shoumeng Yan, and Changshui Zhang. Learning efficient convolutional networks through network slimming. In *Proceedings of the IEEE international conference on computer vision*, pages 2736–2744, 2017. [2](#)
- [23] Jian-Hao Luo, Jianxin Wu, and Weiyao Lin. Thinet: A filter level pruning method for deep neural network compression. In *Proceedings of the IEEE international conference on computer vision*, pages 5058–5066, 2017. [2](#)
- [24] Jiageng Mao, Xiaogang Wang, and Hongsheng Li. Interpolated convolutional networks for 3d point cloud understanding. In *Proceedings of the IEEE/CVF International Conference on Computer Vision*, pages 1578–1587, 2019. [1](#), [2](#), [3](#)
- [25] Lars Mescheder, Michael Oechsle, Michael Niemeyer, Sebastian Nowozin, and Andreas Geiger. Occupancy networks: Learning 3d reconstruction in function space. In *Proceedings of the IEEE/CVF Conference on Computer Vision and Pattern Recognition*, pages 4460–4470, 2019. [1](#)
- [26] Pavlo Molchanov, Stephen Tyree, Tero Karras, Timo Aila, and Jan Kautz. Pruning convolutional neural networks for resource efficient inference. *arXiv preprint arXiv:1611.06440*, 2016. [1](#), [2](#), [4](#)
- [27] Michael C Mozer and Paul Smolensky. Skeletonization: A technique for trimming the fat from a network via relevance assessment. In *Advances in neural information processing systems*, pages 107–115, 1989. [1](#)

- [28] Alexey Nekrasov, Jonas Schult, Or Litany, Bastian Leibe, and Francis Engelmann. Mix3d: Out-of-context data augmentation for 3d scenes. *arXiv preprint arXiv:2110.02210*, 2021. 4
- [29] Adam Paszke, Sam Gross, Francisco Massa, Adam Lerer, James Bradbury, Gregory Chanan, Trevor Killeen, Zeming Lin, Natalia Gimelshein, Luca Antiga, Alban Desmaison, Andreas Kopf, Edward Yang, Zachary DeVito, Martin Raison, Alykhan Tejani, Sasank Chilamkurthy, Benoit Steiner, Lu Fang, Junjie Bai, and Soumith Chintala. Pytorch: An imperative style, high-performance deep learning library. In H. Wallach, H. Larochelle, A. Beygelzimer, F. d'Alché-Buc, E. Fox, and R. Garnett, editors, *Advances in Neural Information Processing Systems 32*, pages 8024–8035. Curran Associates, Inc., 2019. 5
- [30] Charles R Qi, Or Litany, Kaiming He, and Leonidas J Guibas. Deep hough voting for 3d object detection in point clouds. In *Proceedings of the IEEE/CVF International Conference on Computer Vision*, pages 9277–9286, 2019. 1
- [31] Charles R Qi, Hao Su, Kaichun Mo, and Leonidas J Guibas. Pointnet: Deep learning on point sets for 3d classification and segmentation. In *Proceedings of the IEEE conference on computer vision and pattern recognition*, pages 652–660, 2017. 1, 2, 3, 5, 6, 7
- [32] Charles R Qi, Li Yi, Hao Su, and Leonidas J Guibas. Pointnet++: Deep hierarchical feature learning on point sets in a metric space. *arXiv preprint arXiv:1706.02413*, 2017. 1, 2, 3, 5, 6, 7
- [33] Olaf Ronneberger, Philipp Fischer, and Thomas Brox. U-net: Convolutional networks for biomedical image segmentation. In *International Conference on Medical image computing and computer-assisted intervention*, pages 234–241. Springer, 2015. 2
- [34] Pei Sun, Henrik Kretschmar, Xerxes Dotiwalla, Aurelien Chouard, Vijaysai Patnaik, Paul Tsui, James Guo, Yin Zhou, Yuning Chai, Benjamin Caine, et al. Scalability in perception for autonomous driving: Waymo open dataset. In *Proceedings of the IEEE/CVF Conference on Computer Vision and Pattern Recognition*, pages 2446–2454, 2020. 1
- [35] Mingxing Tan and Quoc Le. Efficientnet: Rethinking model scaling for convolutional neural networks. In *International Conference on Machine Learning*, pages 6105–6114. PMLR, 2019. 2
- [36] Hidenori Tanaka, Daniel Kunin, Daniel LK Yamins, and Surya Ganguli. Pruning neural networks without any data by iteratively conserving synaptic flow. *arXiv preprint arXiv:2006.05467*, 2020. 3
- [37] Maxim Tatarchenko, Jaesik Park, Vladlen Koltun, and Qian-Yi Zhou. Tangent convolutions for dense prediction in 3d. In *Proceedings of the IEEE Conference on Computer Vision and Pattern Recognition*, pages 3887–3896, 2018. 1, 2, 5, 6
- [38] Hugues Thomas, Charles R Qi, Jean-Emmanuel Deschaud, Beatriz Marcotegui, François Goulette, and Leonidas J Guibas. Kpconv: Flexible and deformable convolution for point clouds. In *Proceedings of the IEEE/CVF International Conference on Computer Vision*, pages 6411–6420, 2019. 1, 2, 3, 5, 6
- [39] Chaoqi Wang, Guodong Zhang, and Roger Grosse. Picking winning tickets before training by preserving gradient flow. *arXiv preprint arXiv:2002.07376*, 2020. 3
- [40] Yue Wang, Yongbin Sun, Ziwei Liu, Sanjay E Sarma, Michael M Bronstein, and Justin M Solomon. Dynamic graph cnn for learning on point clouds. *Acm Transactions On Graphics (tog)*, 38(5):1–12, 2019. 1, 2
- [41] Zhenzhen Wang, Weixiang Hong, Yap-Peng Tan, and Jun-song Yuan. Pruning 3d filters for accelerating 3d convnets. *IEEE Transactions on Multimedia*, 22(8):2126–2137, 2020. 2
- [42] Zhenzhen Wang, Weixiang Hong, Yap-Peng Tan, and Jun-song Yuan. Pruning 3d filters for accelerating 3d convnets. *IEEE Transactions on Multimedia*, 22(8):2126–2137, 2020. 3
- [43] Wenxuan Wu, Zhongang Qi, and Li Fuxin. Pointconv: Deep convolutional networks on 3d point clouds. In *Proceedings of the IEEE/CVF Conference on Computer Vision and Pattern Recognition*, pages 9621–9630, 2019. 5, 6
- [44] Mutian Xu, Runyu Ding, Hengshuang Zhao, and Xiaojuan Qi. Paconv: Position adaptive convolution with dynamic kernel assembling on point clouds. In *Proceedings of the IEEE/CVF Conference on Computer Vision and Pattern Recognition*, pages 3173–3182, 2021. 3, 5, 6
- [45] Xu Yan, Chaoda Zheng, Zhen Li, Sheng Wang, and Shuguang Cui. Pointasnl: Robust point clouds processing using nonlocal neural networks with adaptive sampling. In *Proceedings of the IEEE/CVF Conference on Computer Vision and Pattern Recognition*, pages 5589–5598, 2020. 5, 6
- [46] Xiangyu Zhang, Xinyu Zhou, Mengxiao Lin, and Jian Sun. Shufflenet: An extremely efficient convolutional neural network for mobile devices. In *Proceedings of the IEEE conference on computer vision and pattern recognition*, pages 6848–6856, 2018. 2
- [47] Hengshuang Zhao, Li Jiang, Jiaya Jia, Philip HS Torr, and Vladlen Koltun. Point transformer. In *Proceedings of the IEEE/CVF International Conference on Computer Vision*, pages 16259–16268, 2021. 1, 2, 3, 5, 6
- [48] Hattie Zhou, Janice Lan, Rosanne Liu, and Jason Yosinski. Deconstructing lottery tickets: Zeros, signs, and the supermask. *arXiv preprint arXiv:1905.01067*, 2019. 3, 4, 5

## A. Appendix

In this appendix, we provide additional details and results of our method.

### A.1. Architecture details

For all experiments, we used three baseline networks for network compression and analysis. We provide the architectural details of these networks. As illustrated in Table a.1, the networks share the same backbone but have varying depths and widths. The backbone has four steps of downsampling and upsampling using convolution and transposed convolution layers with stride 2. Hence, at the very bottom of the bottleneck, the resolution of an input voxel reduces 16 times than its initial value. In total, there are 8 residual blocks between upsampling and downsampling. Between the same upsampled and downsampled features with the same resolution, it has skip connections. For semantic segmentation, the features are projected to logits using  $1 \times 1 \times 1$  convolution layer with  $N_C$  output dimension, where  $N_C = 20$  for ScanNet [6] and 13 for S3DIS [1]. Note that instance segmentation models have an additional head for predicting the offset coordinates for instance centroids.

### A.2. Additional analysis of pruning criteria.

In Figure a.1, we visualize the performance vs. model size graphs on S3DIS semantic segmentation (left), ScanNet instance segmentation (middle), and S3DIS instance segmentation (right). For semantic segmentation model, we use mIoU for our main performance metric; for instance segmentation, we use mAP50 for our evaluation metric.

We found that the global pruning strategies show better pruning efficiency than the local pruning methods across all datasets and tasks. Note that in the S3DIS instance segmentation experiment, some pruning strategies show the best performance on a 95% pruned model, not on 90% pruned models. We speculate that the 95% pruned model generalizes better than the larger 90% pruned models because the instance segmentation task on S3DIS is monotonic and lacks diversity compared with the ScanNet dataset.

### A.3. Additional kernel visualization.

In Figure a.2, we visualize the compressed convolution kernels with different pruning strategies, or different compression rates. All models are Res16UNet34C trained and pruned on ScanNet semantic segmentation.

As shown in the figure, all pruning strategies tend to prune the weights of decoder more aggressively. While the models pruned with global pruning methods have relatively dense encoders, the local pruning methods make the encoder sparser. Furthermore, we identify that the pattern of convolution kernels, alignment along the gravity axis, reveals as the model is compressed more significantly.

### A.4. Additional qualitative results.

We provide additional visualizations of semantic segmentation results on the S3DIS dataset (Figure a.3), instance segmentation on the ScanNet dataset (Figure a.4), and instance segmentation on the S3DIS dataset (Figure a.5). We use compressed Res16UNet34C models for all experiments.

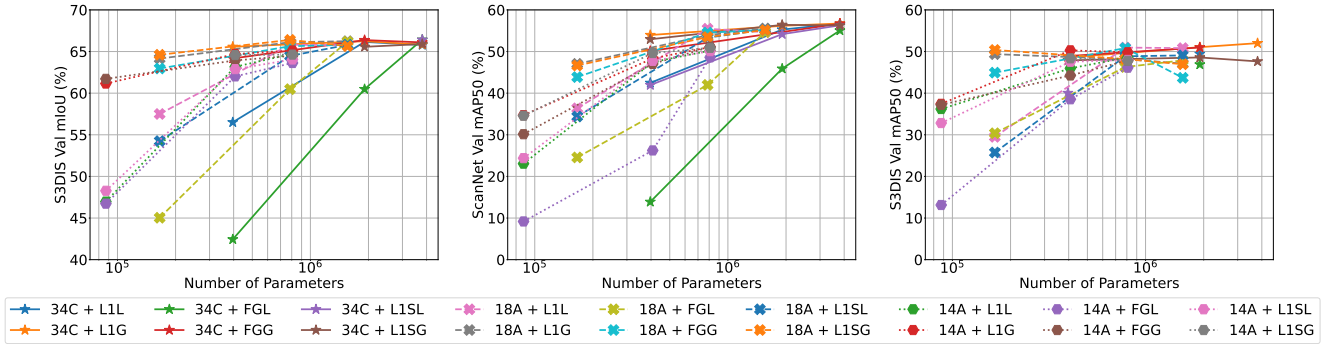


Figure a.1. Ablation study on different pruning criteria on S3DIS [1] semantic segmentation (Left), ScanNet [6] instance segmentation (Middle), and S3DIS instance segmentation (Right).

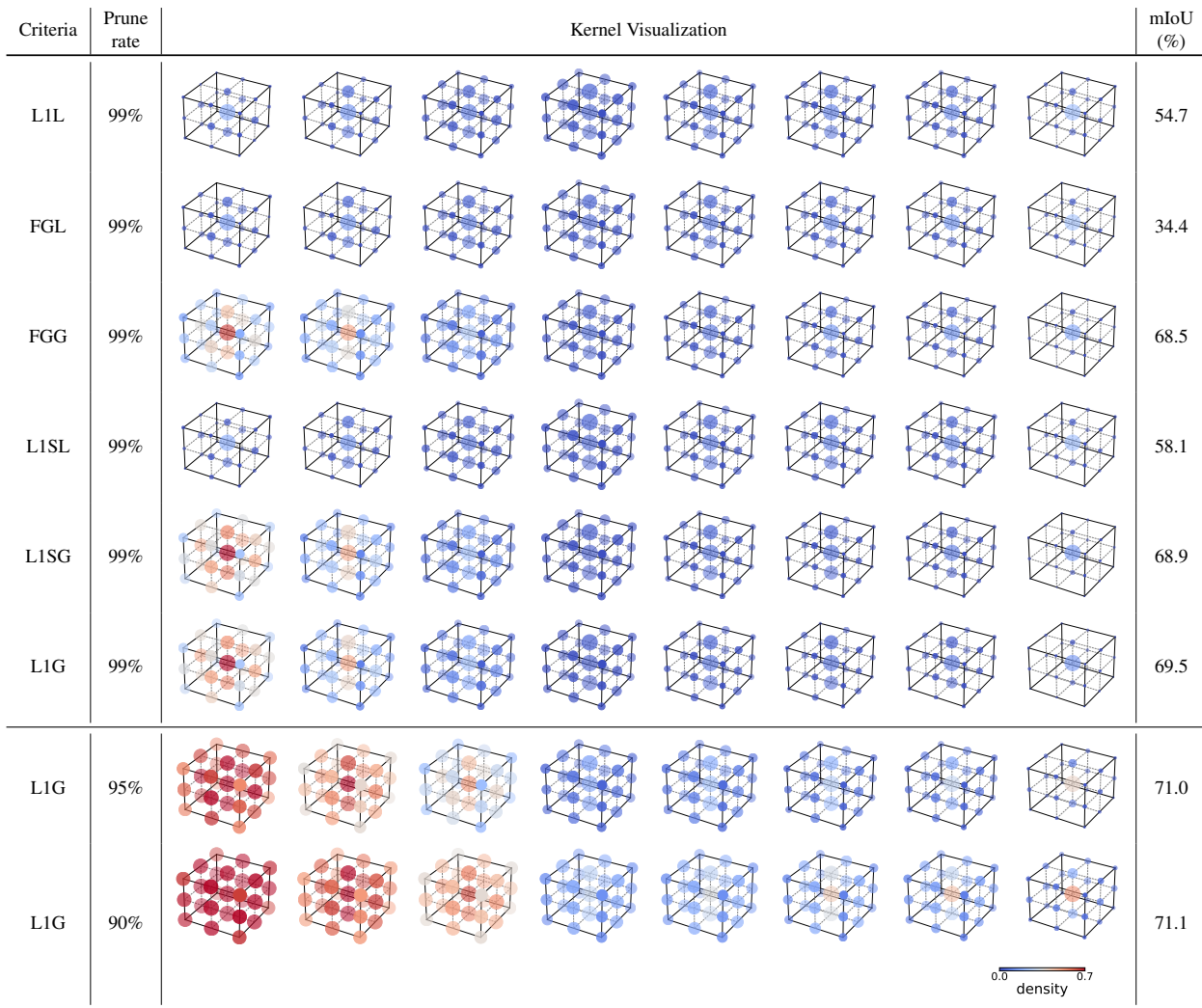
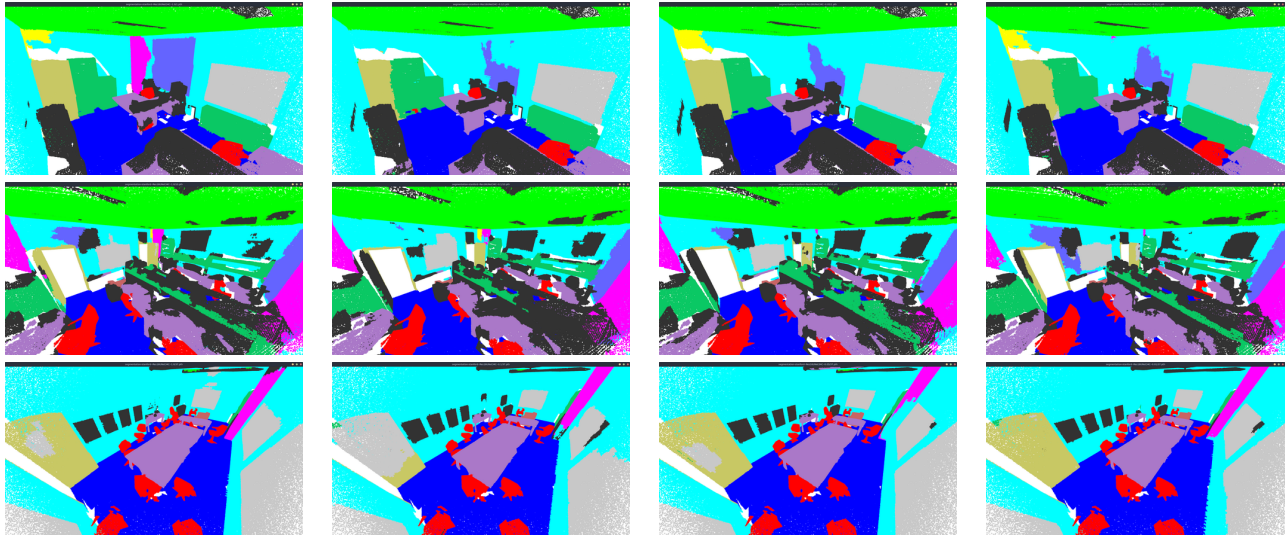


Figure a.2. Visualizations of compressed convolution kernels. We use Res16UNet34C for all kernel visualizations. We present convolution kernels compressed with different pruning criteria on the first 6 rows, and kernels compressed with different compression rate on the last three rows.

layer name	Res16UNet14A	Res16UNet18A	Res16UNet34C
conv0	$3 \times 3 \times 3, 32$		
conv1	$2 \times 2 \times 2, 32, \text{stride } 2$		
block1	$\begin{bmatrix} 3 \times 3 \times 3, 32 \\ 3 \times 3 \times 3, 32 \end{bmatrix} \times 1$	$\begin{bmatrix} 3 \times 3 \times 3, 32 \\ 3 \times 3 \times 3, 32 \end{bmatrix} \times 2$	$\begin{bmatrix} 3 \times 3 \times 3, 32 \\ 3 \times 3 \times 3, 32 \end{bmatrix} \times 2$
conv2	$2 \times 2 \times 2, 32, \text{stride } 2$		
block2	$\begin{bmatrix} 3 \times 3 \times 3, 64 \\ 3 \times 3 \times 3, 64 \end{bmatrix} \times 1$	$\begin{bmatrix} 3 \times 3 \times 3, 64 \\ 3 \times 3 \times 3, 64 \end{bmatrix} \times 2$	$\begin{bmatrix} 3 \times 3 \times 3, 64 \\ 3 \times 3 \times 3, 64 \end{bmatrix} \times 3$
conv3	$2 \times 2 \times 2, 64, \text{stride } 2$		
block3	$\begin{bmatrix} 3 \times 3 \times 3, 128 \\ 3 \times 3 \times 3, 128 \end{bmatrix} \times 1$	$\begin{bmatrix} 3 \times 3 \times 3, 128 \\ 3 \times 3 \times 3, 128 \end{bmatrix} \times 2$	$\begin{bmatrix} 3 \times 3 \times 3, 128 \\ 3 \times 3 \times 3, 128 \end{bmatrix} \times 4$
conv4	$2 \times 2 \times 2, 128, \text{stride } 2$		
block4	$\begin{bmatrix} 3 \times 3 \times 3, 256 \\ 3 \times 3 \times 3, 256 \end{bmatrix} \times 1$	$\begin{bmatrix} 3 \times 3 \times 3, 256 \\ 3 \times 3 \times 3, 256 \end{bmatrix} \times 2$	$\begin{bmatrix} 3 \times 3 \times 3, 256 \\ 3 \times 3 \times 3, 256 \end{bmatrix} \times 6$
conv4_tr	$2 \times 2 \times 2, 128, \text{stride } 2$		$2 \times 2 \times 2, 256, \text{stride } 2$
block5	$\begin{bmatrix} 3 \times 3 \times 3, 128 \\ 3 \times 3 \times 3, 128 \end{bmatrix} \times 1$	$\begin{bmatrix} 3 \times 3 \times 3, 128 \\ 3 \times 3 \times 3, 128 \end{bmatrix} \times 2$	$\begin{bmatrix} 3 \times 3 \times 3, 256 \\ 3 \times 3 \times 3, 256 \end{bmatrix} \times 2$
conv5_tr	$2 \times 2 \times 2, 128, \text{stride } 2$		
block6	$\begin{bmatrix} 3 \times 3 \times 3, 128 \\ 3 \times 3 \times 3, 128 \end{bmatrix} \times 1$	$\begin{bmatrix} 3 \times 3 \times 3, 128 \\ 3 \times 3 \times 3, 128 \end{bmatrix} \times 2$	$\begin{bmatrix} 3 \times 3 \times 3, 128 \\ 3 \times 3 \times 3, 128 \end{bmatrix} \times 2$
conv6_tr	$2 \times 2 \times 2, 96, \text{stride } 2$		
block7	$\begin{bmatrix} 3 \times 3 \times 3, 96 \\ 3 \times 3 \times 3, 96 \end{bmatrix} \times 1$	$\begin{bmatrix} 3 \times 3 \times 3, 96 \\ 3 \times 3 \times 3, 96 \end{bmatrix} \times 2$	$\begin{bmatrix} 3 \times 3 \times 3, 96 \\ 3 \times 3 \times 3, 96 \end{bmatrix} \times 2$
conv7_tr	$2 \times 2 \times 2, 96, \text{stride } 2$		
block8	$\begin{bmatrix} 3 \times 3 \times 3, 96 \\ 3 \times 3 \times 3, 96 \end{bmatrix} \times 1$	$\begin{bmatrix} 3 \times 3 \times 3, 96 \\ 3 \times 3 \times 3, 96 \end{bmatrix} \times 2$	$\begin{bmatrix} 3 \times 3 \times 3, 96 \\ 3 \times 3 \times 3, 96 \end{bmatrix} \times 2$
final	$1 \times 1 \times 1, N_C$		
offset*	$\begin{bmatrix} 1 \times 1 \times 1, 96 \\ 1 \times 1 \times 1, 3 \end{bmatrix}$		
Number of Params	$8.02 \times 10^6$	$15.5 \times 10^6$	$37.9 \times 10^6$

Table a.1. Architectures of Res16UNet variants. We denote a convolution layer with its kernel size, output channel size, and convolution stride size. If a stride side is not specified, it is assumed that there is no stride. All convolution layers except for the last layer have a Batch Normalization and a ReLU layer after them. The layers with the tag "conv\_tr" indicates the transposed convolution layers. We use a square bracket to denote a residual block, with the number of blocks stacked. For instance segmentation, the additional head (offset\*) for offset estimation exists, as depicted in Figure 2 (Top) in our main paper.



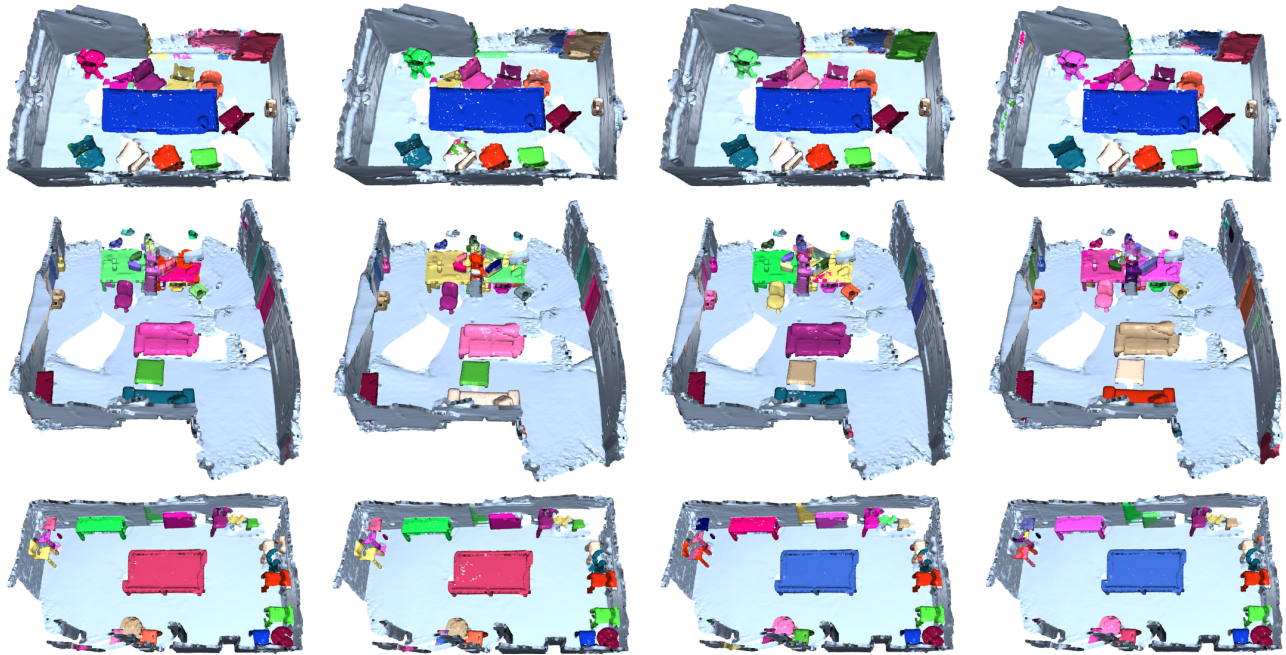
(a) Reference Network  
(Res16UNet34C)

(b) 90% pruned

(c) 95% pruned

(d) 99% pruned

Figure a.3. Semantic segmentation qualitative results on S3DIS [1].



(a) Reference Network  
(Res16UNet34C)

(b) 90% pruned

(c) 95% pruned

(d) 99% pruned

Figure a.4. Instance segmentation qualitative results on ScanNet [6].

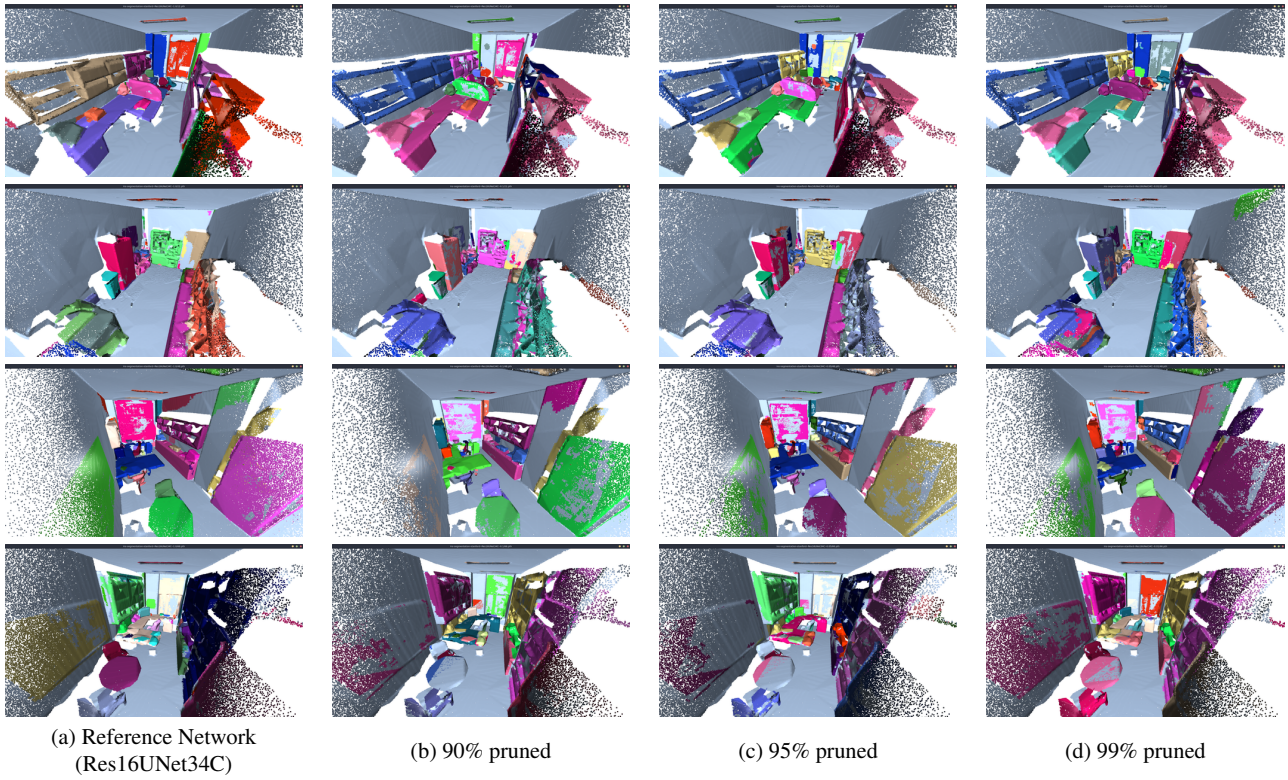


Figure a.5. Instance segmentation qualitative results on S3DIS [1].